Article

Photocatalytic Reduction of Cr(VI) to Cr(III) and Photocatalytic Degradation of Methylene Blue and Antifungal Activity of Ag/TiO₂ Composites Synthesized via the Template Induced Route

Zunaira Zahid [1], Abdul Rauf [1,*], Mohsin Javed [1], Ahmad Alhujaily [2], Shahid Iqbal [3,*], Adnan Amjad [1], Muhammad Arif [1], Sajjad Hussain [4], Ali Bahadur [5], Nasser S. Awwad [6], Hala A. Ibrahium [7,8], Foziah F. Al-Fawzan [9] and Eslam B. Elkaeed [10]

[1] Department of Chemistry, University of Management and Technology, Lahore 54770, Pakistan
[2] Biology Department, College of Science, Taibah University, Al Madinah Al Munawarah 41477, Saudi Arabia
[3] Department of Chemistry, School of Natural Sciences (SNS), National University of Science and Technology (NUST), H-12, Islamabad 46000, Pakistan
[4] School of Chemistry, Faculty of Basic Sciences and Mathematics, Minhaj University, Lahore 54000, Pakistan
[5] Department of Chemistry, College of Science and Technology, Wenzhou-Kean University, Wenzhou 325060, China
[6] Chemistry Department, Faculty of Science, King Khalid University, P.O. Box 9004, Abha 61413, Saudi Arabia
[7] Biology Department, Faculty of Science, King Khalid University, P.O. Box 9004, Abha 61413, Saudi Arabia
[8] Department of Semi Pilot Plant, Nuclear Materials Authority, P.O. Box 530, El-Maadi, Cairo 11381, Egypt
[9] Department of Chemistry, College of Science, Princess Nourah bint Abdulrahman University, P.O. Box 84428, Riyadh 11671, Saudi Arabia
[10] Department of Pharmaceutical Sciences, College of Pharmacy, AlMaarefa University, Riyadh 13713, Saudi Arabia
* Correspondence: abdulrauf@umt.edu.pk (A.R.); shahidgcs10@yahoo.com (S.I.)

Abstract: Water treatment through photocatalysts has become an important topic regarding environmental protection. In the present study, silver and TiO₂ (Ag/TiO₂) composites for photocatalysts were effectively synthesized by adopting the template induced method. The prepared samples were characterized using XRD, FTIR spectroscopy, SEM, and EDX. The constructed samples' particle size and shape were evaluated using a SEM, and the XRD patterns showed anatase crystalline phases. Their morphologies were controllable with changing concentration of reactants and calcination temperature. The synthesized composites act as catalyst in the degradation of methylene blue (MB) and reduction of Cr(VI) to Cr(III) under solar irradiation. In both of these activities, the best result has been shown by the 0.01 Ag/TiO₂ composite. Methanol is used as the hole scavenger in the reduction of Cr(VI) to Cr(III). While the pH factor is important in the photocatalytic reduction of Cr(VI) to Cr(III). According to observations, *S. macrospora and S. maydis* were each subject to 0.01 Ag/TiO₂ nanocomposites maximum antifungal activity, which was 38.4 mm and 34.3 mm, respectively. The outcomes demonstrate that both photocatalytic and antifungal properties are effectively displayed by the constructed material.

Keywords: Ag/TiO₂ composites; template induced method; methylene blue; Cr(VI); photocatalytic reduction; antifungal

1. Introduction

The earth is immensely affected by wastewater management, environmental pollution, and climate change crisis. The major portion of the earth is comprised of water that can be regenerated, disseminated, distributed, and transported. These characteristics collectively add to water's great value to people [1–3]. The groundwater and surface water resources are crucial for a variety of activities, including cattle development, energy generation,

forestry, farming, aquaculture, seafaring, recreation, and so forth [4]. It is a remarkable gift from the nature to humanity that must be preserved. However, environmental degradation, particularly water contamination, is regarded as one of the fundamental issues facing the entire planet, significantly affecting our everyday lives [5]. It comprises the introduction of foreign chemicals into the environment, which harms and disturbs the biosphere [6]. These pollutants appear to be either native substances that have surpassed permitted limits or foreign compounds [7–10]. Unfortunately, pollution is continually rising and is now a severe issue that requires immediate attention [11]. The usage of dyes and their byproducts significantly pollutes the environment. The nature of water is changed by its release of chemicals from potable to non-potable [12]. Furthermore, microorganisms also change the properties of water and cause different diseases. Many nanomaterials have significant properties to control the growth of bacteria [13]. The aquatic center is unscrewed from the dye waste, changing the soil's composition and water content. In addition, it encourages several illnesses, environmental degradation, and several infectious diseases.

Toxic metal and organic compound-related water contamination is still a significant environmental and societal issue [14]. Additionally, water contamination has grown to be a significant cause of worry and a top priority for most industrial sectors. Water contamination is significantly influenced by dyes used in the paper, food, and textile sectors. Due to their industrial use, dyes and associated hydrocarbons, which are among the most significant and dangerous toxins in water, are linked to population expansion [15]. Because dyes have chromophore groups in their structure, they are utilized in coloring fabrics. These colors may be distinguished from one another by how easily they dissolve in water. Most dyes are categorized according to the fibers they will be imprinted on and their chemical and physical makeup. MB (methylene blue) is used to tone down the hues of silk in addition to dying paper and office supplies [16]. MB poses a significant concern to human health and can have a negative impact on the environment because it is poisonous, carcinogenic, and non-biodegradable [17–19]. The health of people can be seriously harmed by color molecules at extremely low concentrations [20]. It can result in eye burns, which may result in both human and animal eyes being permanently damaged. When ingested through the mouth, it generates a burning feeling and may cause vomiting, excessive perspiration [21], methemoglobinemia [22], and mental disorientation [23]. It can also cause short periods of rapid or difficult breathing when inhaled.

Heavy metals also play a vital role in polluting and poisoning the water. In water, the presence of heavy metals even in a very low concentration is considered to be poisonous and the high specific density and atomic weight of the metalloids make them dangerous [24]. Additionally, such contamination can result in several "neurological, cardiovascular, hematological, respiratory and renal problems" that also impact the bladder, lungs, liver, and kidneys [25]. Although there are naturally occurring heavy metals in the ecosystem, man-made sources of heavy metals are the fourth major cause of pollution. Chromium manganese, copper, arsenic, and lead are the examples of heavy metals that are frequently found in water. Further, chromium is frequently employed in many industrial processes, including the production of paint and metal plating [26]. The tanning business utilized between 4.0 and 6.0 thousand tonnes of basic Cr annually, with 20.0 to 40.0% of that amount being disposed of as waste [27]. Cr(VI) is on the list of priority pollutants in the majority of nations due to its high water mobility and acute toxicity [28]. When compared to Cr, Cr(VI) is 100 times more poisonous (III). Compounds made of Cr(VI) are exceedingly toxic and cancer-causing.

The major reason why chromium(VI) is regarded as being particularly dangerous is that it easily interacts with biological molecules [29]. Due to its low membrane permeability, trivalent chromium Cr(III) is mostly safe in the environment. Chromium in hexavalent form is more effective in piercing the cell membrane through openings for isostructural and isoelectric anions such as HPO_4^{2-} and SO_4^{2-} channels, and these forms of chromium are then raised through phagocytosis [30]. By the adsorption reduction method Cr(VI) is converted into the less toxic form Cr(III) [31]. Hexavalent chromium (Cr(VI)) is the

most toxic heavy metal to living things, and the most potent carcinogen [32]. Dermatitis and recurrent ulcers have been connected to exposure to Cr (VI) [33]. Modern oxidation techniques have proven effective at cleaning industrial effluent [34–36].

The use of solar light in photocatalysis, one of many methods for treating water, has drawn a lot of interest because it is environmentally friendly, economical, and effective in reducing pollutants and energy use [37]. Many commonly used techniques, including coagulation, active carbon adsorption, and precipitation can be utilized to treat wastewater that contains hexavalent chromium. The produced hole and OH$^\bullet$ radical are quickly consumed by sacrificial electron donors such as methanol, preventing the electrons and holes from recombining and making the electrons accessible for the reduction of Cr(VI) [38]. AOPs have a lot of potential for treating industrial waste water that contains dyes because they can degrade soluble organic pollutants in liquid wastes [39]. To remove dye molecules, researchers are now concentrating on heterogeneous catalysts. One of the best AOPs for eliminating organic contaminants from both water and the atmosphere is heterogeneous photocatalysis [40]. Essentially, heterogeneous photocatalysis consists of a catalyst that contain a semiconductor which is activated by using the visible and ultraviolet electromagnetic radiation. The elimination of industrial effluents via the photocatalytic degradation method has attracted interest [41]. By breaking molecular bonds with the species around them, extremely reactive free radicals produced by the photocatalysis process can trigger oxidation–reduction processes, which can reduce or oxidize the pollutants [42]. By inducing radiation, electron and hole pairs are produced on their outer most layers and hydroxyl radical (OH$^\cdot$) and superoxide radical (O$^{\cdot}_2$) are produced by the reaction of water and oxygen with the charge carriers. Due to their potential properties, semiconductor metal oxides (MO) such as SnO_2, CuO, ZnO, and TiO_2, are popular study materials [43–47] such as nonlinear optics [48], photonic crystals [49], electro ceramics components [50], solar cells [51], and gas sensors [52].

By the incorporation of the noble metal nanoparticles in semiconductive oxides, the photocatalytic activity of semiconductors is highly increased [53]. All semiconductors' mechanisms for electron excitation have the potential to lead to electron and hole recombination, which lowers photo-efficiency from the valence band to the conduction band [54]. Noble metals including Au, Ag, Pd, and Pt, can be used to dope TiO_2 because these boost photocatalytic activity by preventing electron–hole pair recombination, which increases photocatalytic activity [55]. Band gap also plays a considerable role in the photocatalytic process [56]. The band gap of the TiO2 is the 3.2 eV. However, when Titina is doped by the noble metal, the band gap decreases. Reduction in the band gap results in an increased photocatalytic degradation and reduction. One of the effective methods to raise TiO_2's photocatalytic effectiveness is to load it with Ag. For water purification silver is doped on the surface of the TiO_2 which acts as the self-cleaning agent. In this way, Ag contributes to the process of photocatalysis. The silver metal acts as electron sinks, making them efficient co-catalysts for boosting TiO_2 photo reactivity. To capture the electrons that are transported from the TiO_2 conduction band, Ag can operate as an electron trap. At the same time, it produces a surface plasmon resonance (SPR) effect, extending the light absorption to the visible spectrum which result in an increase in the photocatalytic performance of TiO_2 [57]. It was discovered that Ag could increase the rate of photocatalytic degradation, facilitate charge separation, and increase the adsorption of organic pollutants on the TiO_2 surface [58]. Ag/TiO_2 also acts as the electron trapping center that prevents the recombination of electrons/holes pairs caused by the Schottky barrier resulting in an enhanced photocatalytic activity [59]. The synergistic impact of Ag, TiO_2, and biochar allowed to effectively manufacture a series of biochar-coupled Ag–TiO_2 materials, and the findings demonstrated that the degradation performance of Ag-modified TiO_2 was better than the pure TiO_2 [60]. Jiang et al. showed that after two hours of exposure to light, doping TiO_2 with silver demonstrated 100% photodegrade performance [61]. According to Arbiter et al. after sixty minutes, silver titanium oxide shows 85% of dye degradation [62]. According to Avciata et al. after 150 min of irritation, 75% dye degradation is shown by the TiO_2 doped

with Ag [63]. Further, the doping of the silver on the TiO_2 also caused the photo reduction of chromium (VI) to the chromium (III). Silver-TiO_2 also acts as the photo catalyst which enhances the reduction of Cr(VI) to Cr(III).

In our continued research work on water pollution, we focus to synthesize the Ag/TiO_2 composites by using the template induce rout for photocatalytic degradation of methylene blue and photocatalytic reduction of Cr (VI) to Cr (III).

2. Experimental Section

2.1. Material and Method

The reactants employed in this investigation included methylene blue (MB), analytical grade sodium carbonate (Na_2CO_3), magnesium chloride ($MgCl_2$), silver nitrate ($AgNO_3$), and potassium dichromate ($K_2Cr_2O_7$). TiO_2 was used as the titania source. X-ray diffraction (XRD) data were obtained employing a Rigaku D-Max 2400 diffractometer operating in reflection mode (Cu-K radiation), and SEM was used to evaluate the produced Ag/TiO_2 composites (FEI Nova Nano SEM 450).

2.2. Preparation of Ag/TiO_2 Composites

The Ag/TiO_2 composites are synthesized by following the template induced route. This is the bottom-up approach for nanotechnology for synthesizing nanomaterials (Figure 1). In this experiment 0.1 M solution of sodium carbonate (Na_2CO_3) and 0.1 M solution of Magnesium chloride ($MgCl_2$) were combined uniformly in a beaker at 40 °C. The aforementioned combination was then mixed at a 400 rpm stirring rate for 7 min, after which the suspension was kept at 80 °C for 4 h. The obtained $Mg_5(CO_3)_4(OH)_2.4H_2O$ product (MCH) was then filtered off, three times washed with first ethanol and then water after being dried at 60 °C for 12 h. After dispersing 1 g of synthetic MCH template in 80 mL of pure ethyl alcohol, TiO_2 was added. The solution of distilled water and ethanol was continuously stirred for 4 h at 25 °C temperature. Deionized water and ethanol were used to wash the MCH/TiO_2 intermediate in succession before it was dried. In 100 mL of absolute ethyl alcohol, 0.8 g of MCH/TiO_2 intermediate was dispersed. The aforesaid combination was then given an adequate amount of $AgNO_3$ solution in three different contents (0.01 M, 0.1 M, and 0.5 M), and the mixture was agitated for two hours. The resultant samples were labeled 0.01-Ag/TiO_2, 0.1-Ag/TiO_2, and 0.5-Ag/TiO_2 with varying concentrations of Ag^+. After bubbling CO_2 gas into the mixture for 30 min to flush out any remaining Mg^{2+} ions, the mixture was once again washed with the buffer solution of CH_3COOH/CH_3COONH_4. This buffer solution is prepared by dissolving 0.1 g ammonium acetate in 10 mL acetic acid. Then the Ag/TiO_2 composites were dried at 60 °C for 12 h. To create Ag/TiO_2 composites, the Ag_2CO_3/TiO_2 precursor was calcined at 550 °C for 4 h.

2.3. Photocatalytic Degradation Experiment

In the photocatalytic degradation experiment, the 0.0006 g methylene blue dye was taken and then added to the 500 mL of water. Afterward, this solution was sonicated for fifteen minutes. Furthermore, three beakers were taken, and 100 mL solution was added to each. About 0.2 g of composite was inserted to every beaker. The solutions were stirred in the absence of light for thirty minutes to achieve adsorption equilibrium. Then, the stired solutions were added to Petri dishes, and 5 mL of the solution was taken as the reference. These Petri dishes were exposed to direct sunlight and 5 mL solution sample was taken at 30, 60, 90, 120, and 150 min respectively. The color of MB faded. The photocatalytic degradation rate can be estimated by using the following equation:
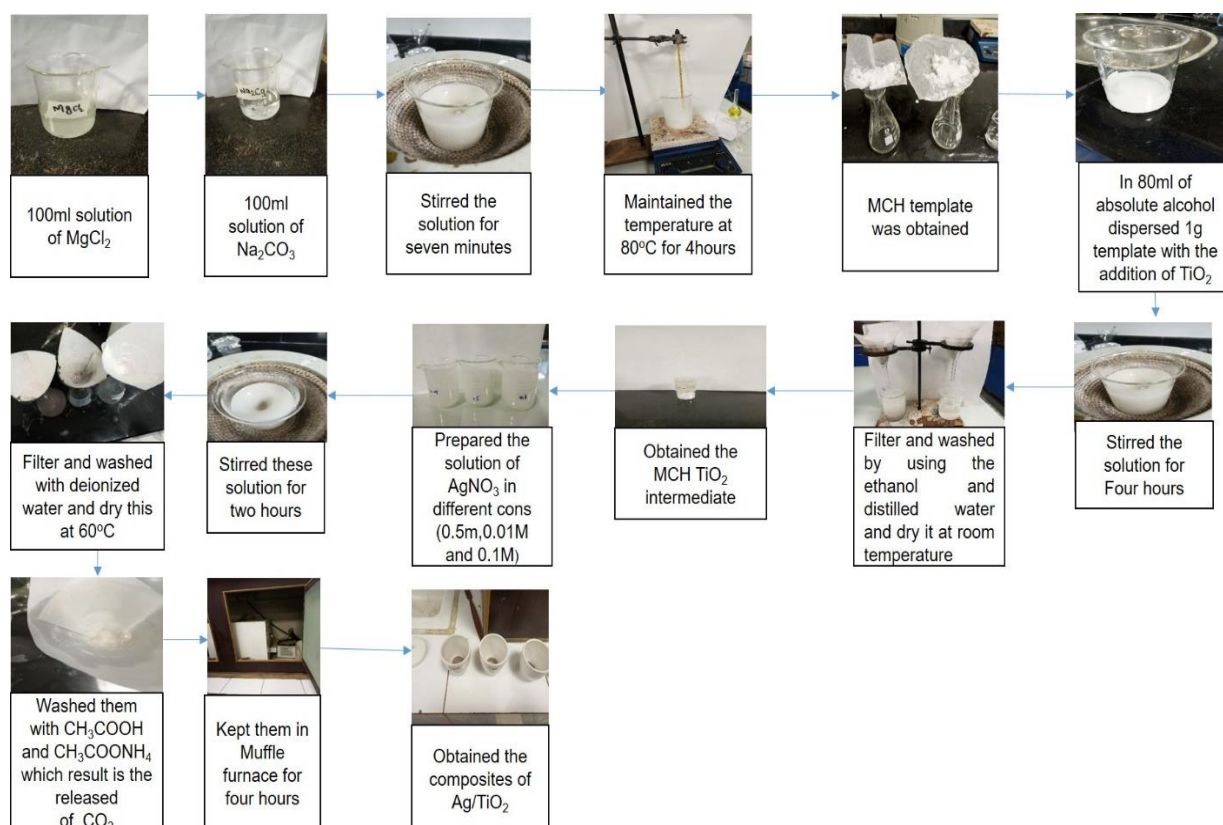
$$Photodegradation\ rate = Co - Ct/Co \times 100$$

Figure 1. Schematic diagram of the synthesis of Ag/TiO$_2$ composites by template induced route.

2.4. Photocatalytic Reduction Experiment

In the photocatalytic reduction experiment, 10 ppm solution of anhydrous K$_2$Cr$_2$O$_7$ was prepared and 0.2 g of 0.01, 0.1, and 0.5 Ag/TiO$_2$ was added to it as a catalyst. Further, 2 ml of methanol was added into the solution which acted as a hole scavenger. The pH of the solution was altered to 1.5 by utilizing NaOH and H$_2$SO$_4$. The solution was stirred for thirty minutes to achieve chemical equilibrium. Taking 0-min reading as the reference afterward, the solutions were poured into a Petri dish and exposed to the sunlight. A total of 5 mL solution was taken in a burette after 5, 10, 15, 20, 15, 20, 25, 30, 35, 40, 45, and 50 min respectively. This experiment was performed in the last days of May. The intensity of the sun was 2100 Wm^2. The removal rate of the chromium can be determined by using the following equation:

$$\text{Photoreduction rate} = Co - Ct/Co \times 100$$

3. Result and Discussion

The FTIR results as shown in Figure 2 revealed that the 3420 cm^{-1} peak relates to the stretching vibration of the hydroxyl group [64]. However, the peak at 1621 cm^{-1} originated due to the bending vibration of the water molecule. The O-Ti-O lattice and Ti-O stretching vibration are responsible for the TiO$_2$ characteristic bands in the range 500–900 cm^{-1}. [*Journal of Materials Science: Materials in Electronics* (2018) 29:18111–18119].

To analyze the crystallinity of Ag/TiO$_2$ composites, XRD was used in the fractional angle range of 10° to 80° as shown in Figure 3. The XRD results show that the peak at 0.01 represents peak a, while the other two peaks represent the peaks of 0.1 and 0.5 given the names b and c respectively. The XRD results of 0.5 Ag/TiO$_2$, 0.1 Ag/TiO$_2$, and 0.01 Ag/TiO$_2$ composites are categorized into two sets. In these two sets, one category shows the peaks of the silver, while all the other peaks are matched with the structure of TiO$_2$ which is present in the rutile phase. The face-centered cube structure of silver is

presented by showing 111, 200, 220, and 311 peaks at definite positions [65]. These peaks are present at the 38.11°, 44.20°, 64.44°, and 77.39° positions [PDF: JCPDS 03–065-2871]. While the other peaks 110,101,210,211,220, 301, and 112 represent the rutile structure of TiO_2. Strong diffraction peaks in XRD patterns at 27°, 36°, and 55° indicated that TiO_2 was in the rutile phase [66]. θ values are 27.3°, 36.0°, 41.0° 54.2°, 56.5°, 68.8°, and 70°, which correspond to tetragonal phase and can be indexed to the [PDF JCPDS 88-1175].
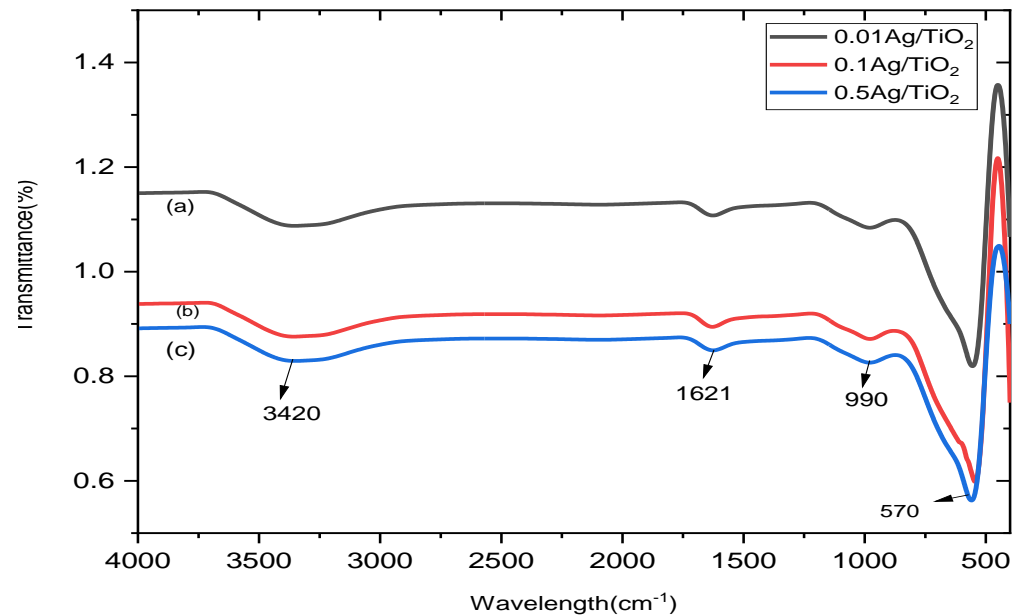
Figure 2. (**a**) FTIR spectrum of 0.01 Ag/TiO_2 composite. (**b**) FTIR spectrum of 0.1 Ag/TiO_2 composite. (**c**) FTIR spectrum of 0.5 Ag/TiO_2.
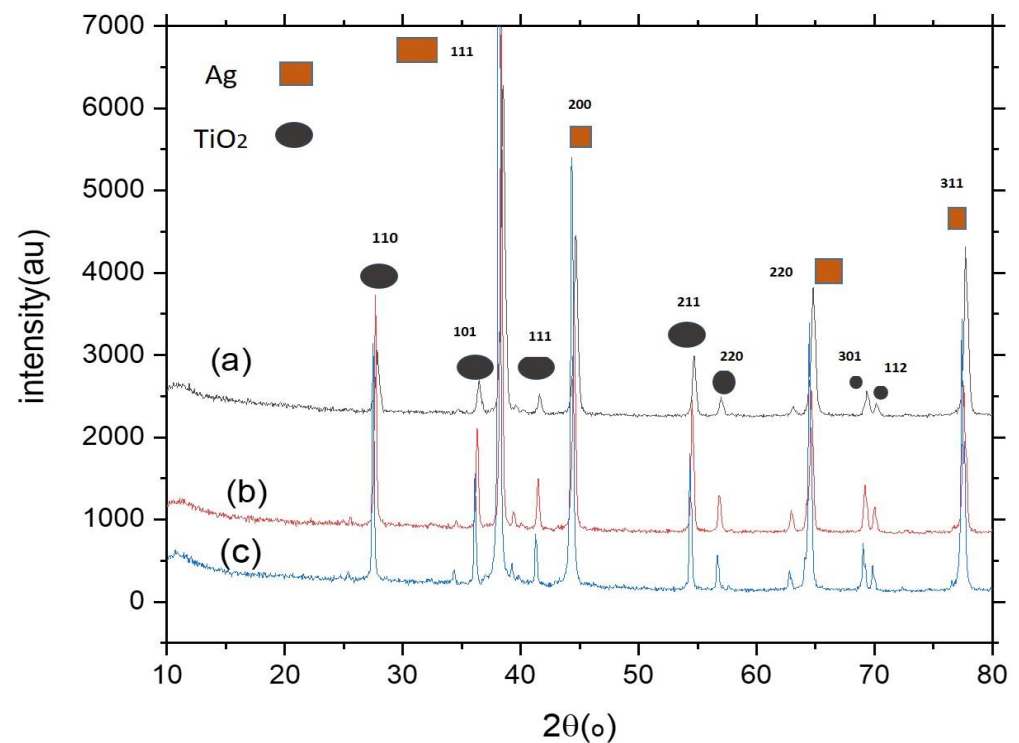

Figure 3. (**a**) XRD of 0.01 Ag/TiO_2 composite. (**b**) XRD of 0.1 Ag/TiO_2 composite. (**c**) XRD of 0.5 Ag/TiO_2 composite.

Figure 4 depicts the scanning and flask-like electron microscope that was used to analyze the Ag/TiO₂ composites' morphology. The shapes of the given images are spherical. Due to spherical shapes, these composites enhance their surface area which increases the capabilities of these composites toward different activities. On the other hand, EDS (Figure 5 and Table 1) showed the Ag element peaks, which demonstrated that Ag was combined within TiO₂.
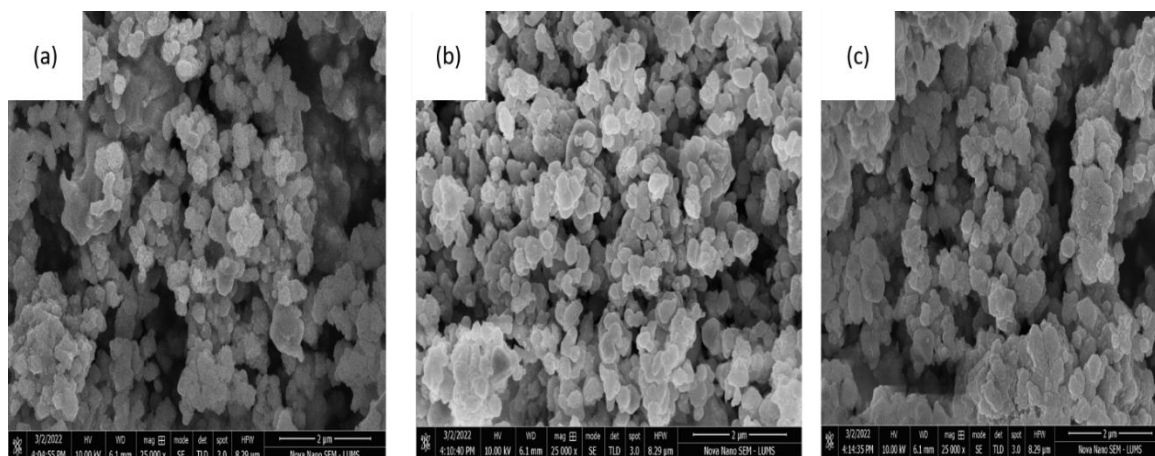

Figure 4. (**a**) SEM image of 0.5 Ag/TiO₂ composite. (**b**) SEM image of 0.01 Ag/TiO₂ composite. (**c**) SEM image of 0.1 Ag/TiO₂ composite.
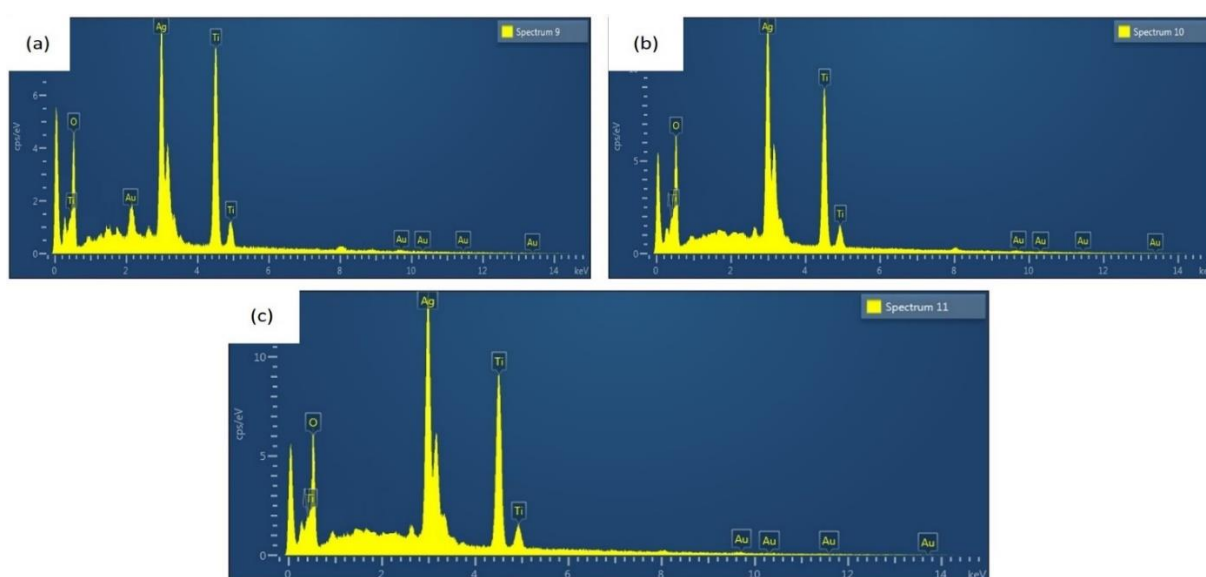

Figure 5. (**a**) EDS of 0.5 Ag/TiO₂ composite. (**b**) EDS of 0.01 Ag/TiO₂ composite. (**c**) EDS of 0.1 Ag/TiO₂ composite.

The morphology of the Ag/TiO₂ composites was examined by using the scanning and flask-like electron microscope. The shapes of the given images are spherical. Due to spherical shapes, these composites enhance their surface area which increases the capabilities of these composites toward different activities.

The smallest amount of energy needed by an electron to break out from its bound state is known as the band gap in Figure 6. Talc plots were created using absorbance data from UV–VIS spectrophotometry at room temperature to calculate the band gap for

manufactured nanoparticles. To do this, relations were used to compute the photon energy "E" and the absorption co-efficient "α" of synthesized samples:

$$E = hv = 1240/\lambda$$

$$\alpha = 4\pi \ (absorbance)/\lambda$$

Table 1. The elemental composition of (**a**) 0.5 Ag/TiO$_2$ composite; (**b**) 0.01 Ag/TiO$_2$ composite; (**c**) 0.1 Ag/TiO$_2$ composite.

| Composite	Element	Line Type	Apparent Concentration	k Ratio	Wt%	Wt% Sigma	Standard Lable	Factory Standard
(a)	O	K series	10.63	0.0357	25.65	0.52	O$_2$	Yes
	Ti	K series	14.32	0.1432	21.19	0.32	Ti	Yes
	Ag	L series	25.29	0.2529	37.96	0.53	Ag	Yes
	Au	M series	2.42	0.0242	4.03	0.24	Au	Yes
(b)	O	K series	10.69	0.0359	26.53	0.55	O$_2$	Yes
	Ti	K series	17.00	0.1700	25.58	0.33	Ti	Yes
	Ag	L series	22.69	0.2268	34.87	0.46	Ag	Yes
	Au	M series	2.75	0.0275	4.69	0.28	Au	Yes
(c)	O	K series	11.58	0.0389	27.23	0.46	O$_2$	Yes
	Ti	K series	14.57	0.1456	21.34	0.28	Ti	Yes
	Ag	L series	24.79	0.2479	36.89	0.46	Ag	Yes
	Au	M series	2.43	0.0242	4.01	0.21	Au	Yes
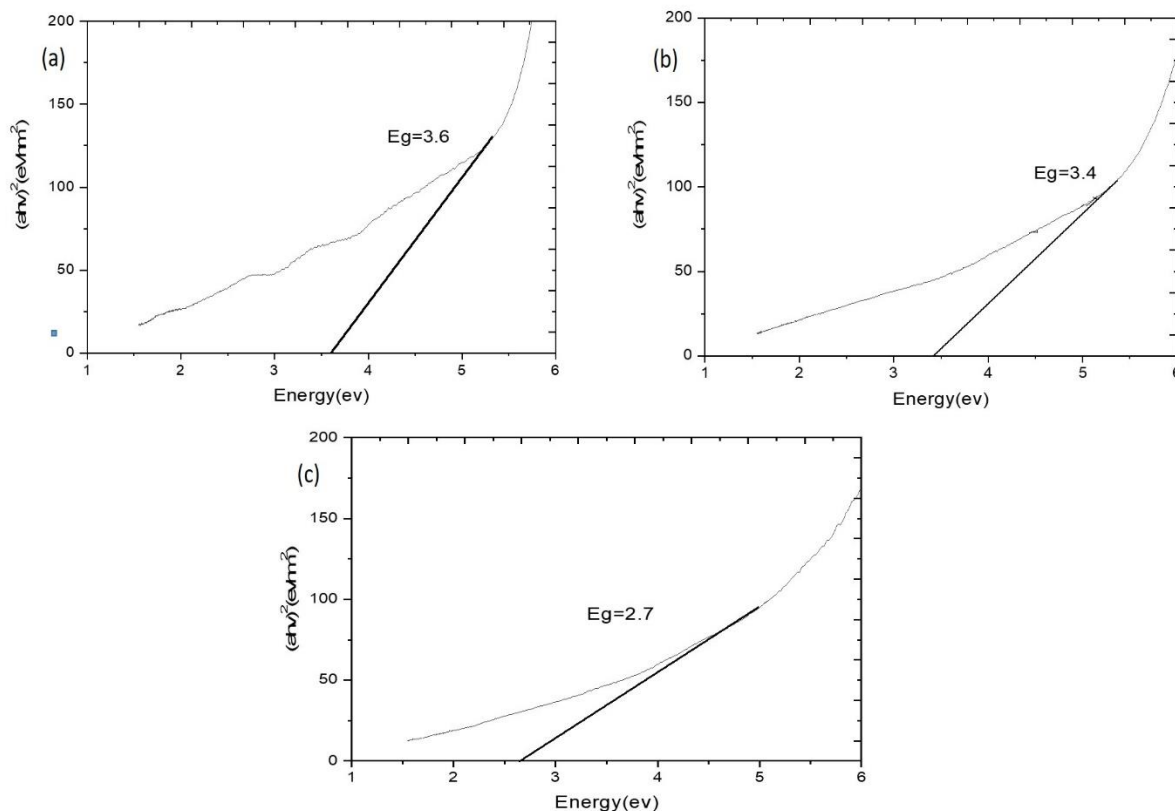
Figure 6. (**a**) Band gap of 0.5 Ag/TiO$_2$ composite. (**b**) Band gap of 0.1 Ag/TiO$_2$ composite. (**c**) Band gap of 0.01 Ag/TiO$_2$ composite.

The absorption coefficient "α" and the energy band gap have the following relation:

$$(\alpha h v) = B\ (h v - H g) 1/2$$

The band gap calculated for the 0.5 Ag/TiO$_2$ composite is 3.6 eV, while for the 0.1 the band gap is 3.4 eV, and for 0.01 Ag/TiO$_2$ composite 2.7 eV.

After exposure to methylene blue under sunlight, degradation of methylene blue started. The readings taken at different time intervals are shown in the Figure 7. After taking the readings at these intervals, the collected solutions were run in a UV-visible spectrophotometer, and the degradation percentage was recorded. After analysis, it was observed that the 0.5 Ag/TiO$_2$, 0.1 Ag/TiO$_2$, and 0.01 Ag/TiO$_2$ composites degraded at 54%, 68%, and 90% respectively. So, the result shows the composite 0.01 Ag/TiO$_2$ shows the highest degradation of methylene blue as compared to the others. Because as the Ag loading exceeds 0.06 wt %, the photocatalytic effectiveness steadily declines, which is mostly caused by the shielding effect of the high Ag coverage.
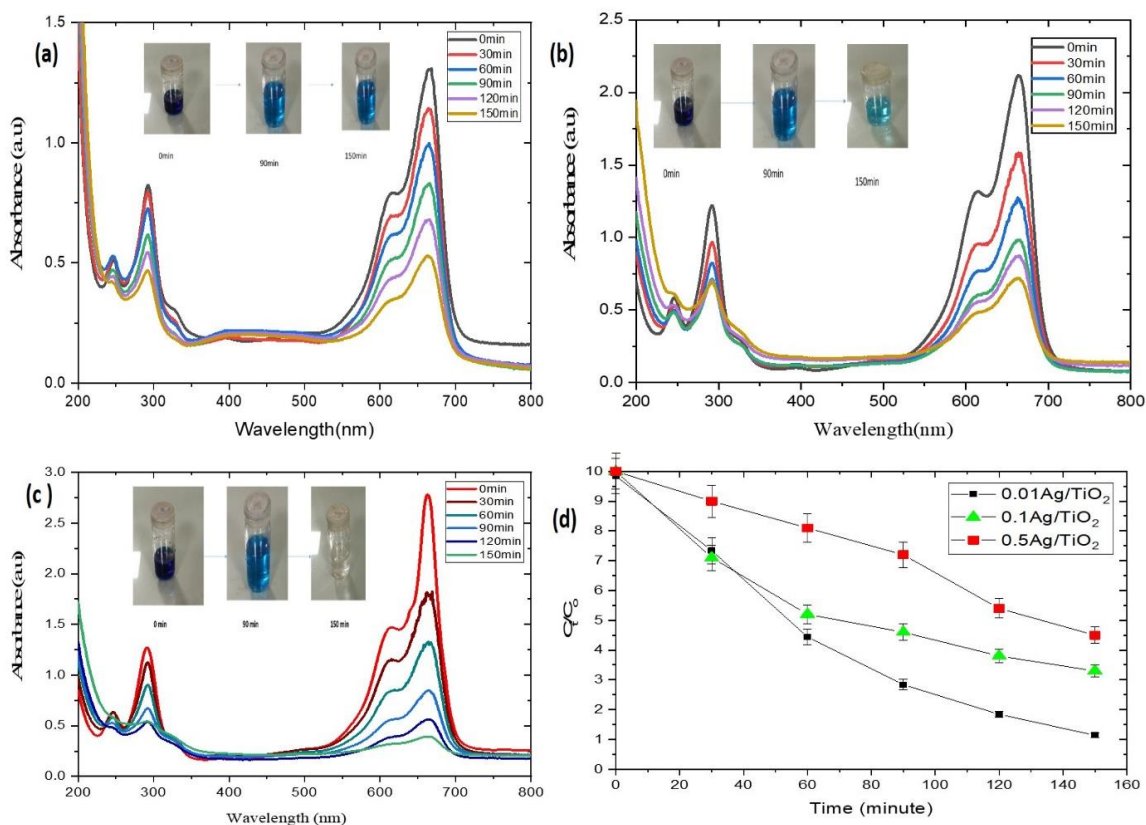

Figure 7. (**a**) The UV visible spectrum of methylene blue in the presence of 0.5 Ag/TiO$_2$ composite. (**b**) In the presence of 0.1 Ag/TiO$_2$ composite, methylene blue's UV spectrum. (**c**) The UV visible spectrum of MB in the presence of 0.01 Ag/TiO$_2$ composite. (**d**) The comparison graph of 0.5 Ag/TiO$_2$, 0.1 Ag/TiO$_2$, and 0.01 Ag/TiO$_2$ composites.

To study the kinetics of the degradation of methylene blue, a graph was plotted between the instantaneous concentration (at radiation time) and the starting concentration of the sample introduced at zero minutes, resulting in a straight line with an R^2 > 0.95 as shown Figure 8 and Table 2. It shows that a first-order reaction was used to quantify the photocatalytic degradation rates for synthesized photocatalysts:

$$-\ln\frac{c_o}{c_t} = kt$$

where c_e is the instantaneous concentration and c_o is the starting concentration of the material being injected at zero minutes (at irradiation of time). While the value of c_t was determined by comparing the Beer–Lamberts Law at zero minutes and at various irradiation times, the value of c_o is known for each photocatalyst.

$$\frac{A}{c} = \frac{\varepsilon}{1}$$

The UV data, as shown in Figure 9, indicate that 50 min of exposure to the sunlight using the 0.5 Ag/TiO$_2$ catalyst results in a 50% reduction of Cr (VI) to Cr (III), while using the 0.1 Ag/TiO$_2$ catalyst shows a 54% reduction of Cr (VI) to Cr (III), and 0.01 Ag/TiO$_2$ composite as the catalyst shows 75% reduction of the Cr (VI) to Cr (III). The pH affects the photoreduction of the Cr (VI) to Cr (III) as shown in Figure 10. The best result is shown by the Ag/TiO$_2$ composites at 1.5 pH as compared to the 5 and 3. So all the experiments of photoreduction of the Cr (VI) to Cr (III) were carried out at pH 1.5.

$$r = -dC/dt = K'C;$$

In the above equation, K', with a unit of time-1, is the fictitious first-order rate constant. r represents the reaction rate where the illumination (reaction) time is represented by t. The amount of aqueous Cr (VI) concentration is denoted by C; where Ce represents the level of Cr (VI) at time t and Co represents the starting level of Cr (VI). The relationship between the Cr (VI) concentration and absorbance is linear as shown in Figure 11 and Table 3 as well.
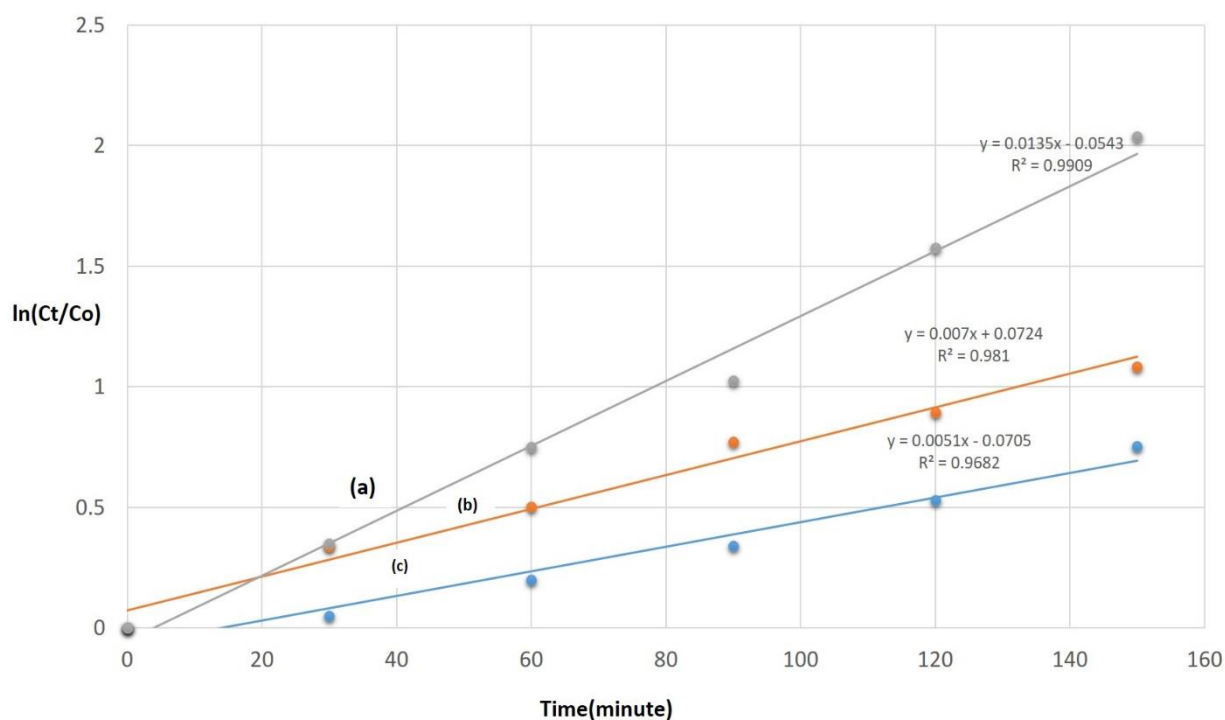
$$\ln (C_t /C_o) = -K'$$

Figure 8. (**a**) The first-order kinetic of 0.01 Ag/TiO$_2$ composite. (**b**) The first-order kinetic of 0.1 Ag/TiO$_2$ composite. (**c**) The first-order kinetic of 0.5 Ag/TiO$_2$ composite.

Table 2. Kinetics study of photocatalytic degradation of methylene blue.

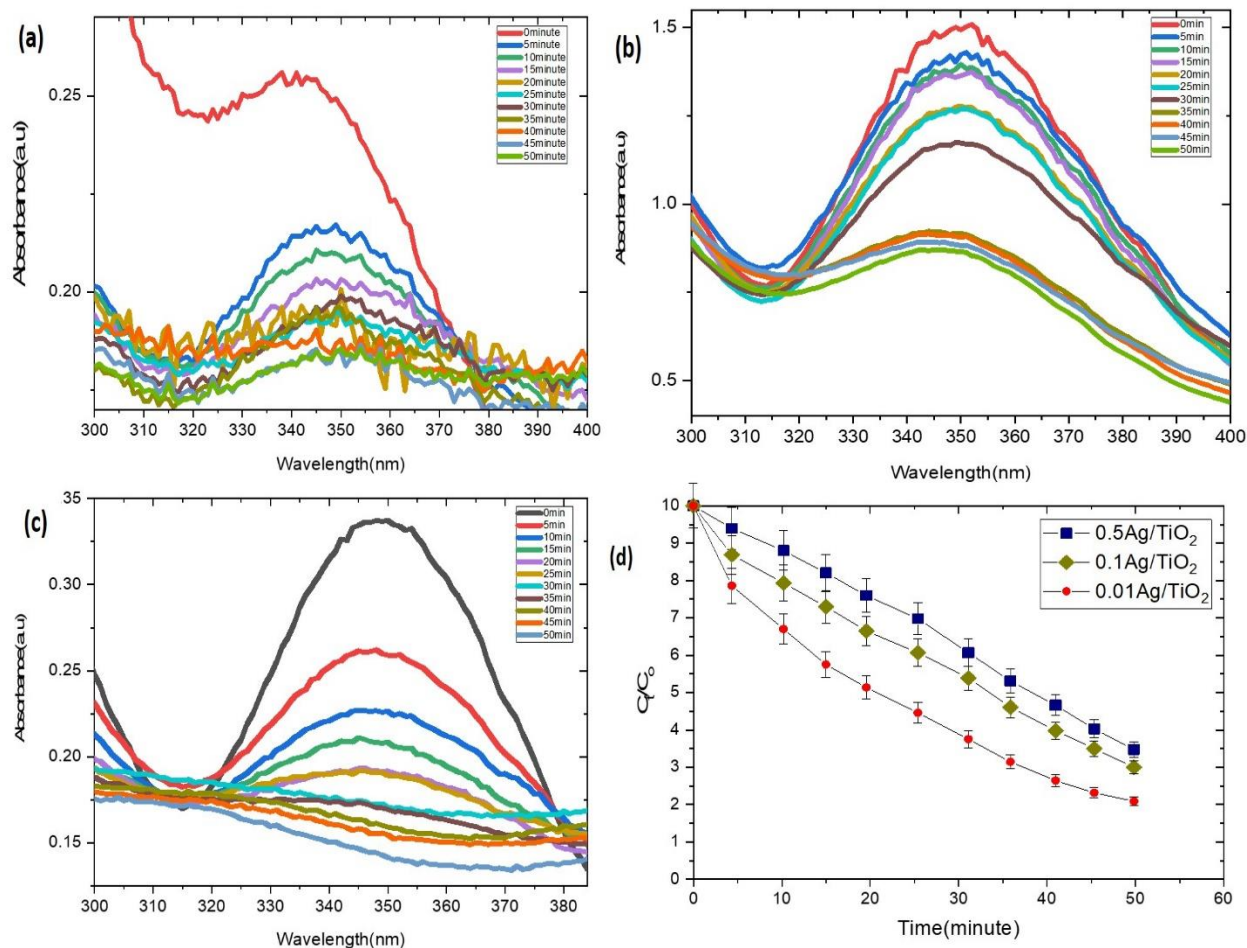| Ag/TiO$_2$ Composites	R^2	K_{app}	Degradation
0.01 Ag/TiO$_2$	0.0090	0.0135	90%
0.1 Ag/TiO$_2$	0.981	0.007	68%
0.5 Ag/TiO$_2$	0.9682	0.0051	54%

Figure 9. (**a**) The UV visible spectra of 0.5 Ag/TiO$_2$ composite of photocatalytic reduction of Cr (VI) to Cr(III). (**b**) The UV visible spectra of 0.1 Ag/TiO$_2$ composite of photocatalytic reduction of Cr(VI) to Cr(III). (**c**) Photocatalytic reduction of Cr(vi) to Cr(III). (**d**) Comparison graph of 0.5 Ag/TiO$_2$, 0.1 Ag/TiO$_2$, and 0.01 Ag/TiO$_2$ composites.

Table 3. Kinetics study of photocatalytic reduction of Cr(VI) to Cr(III).

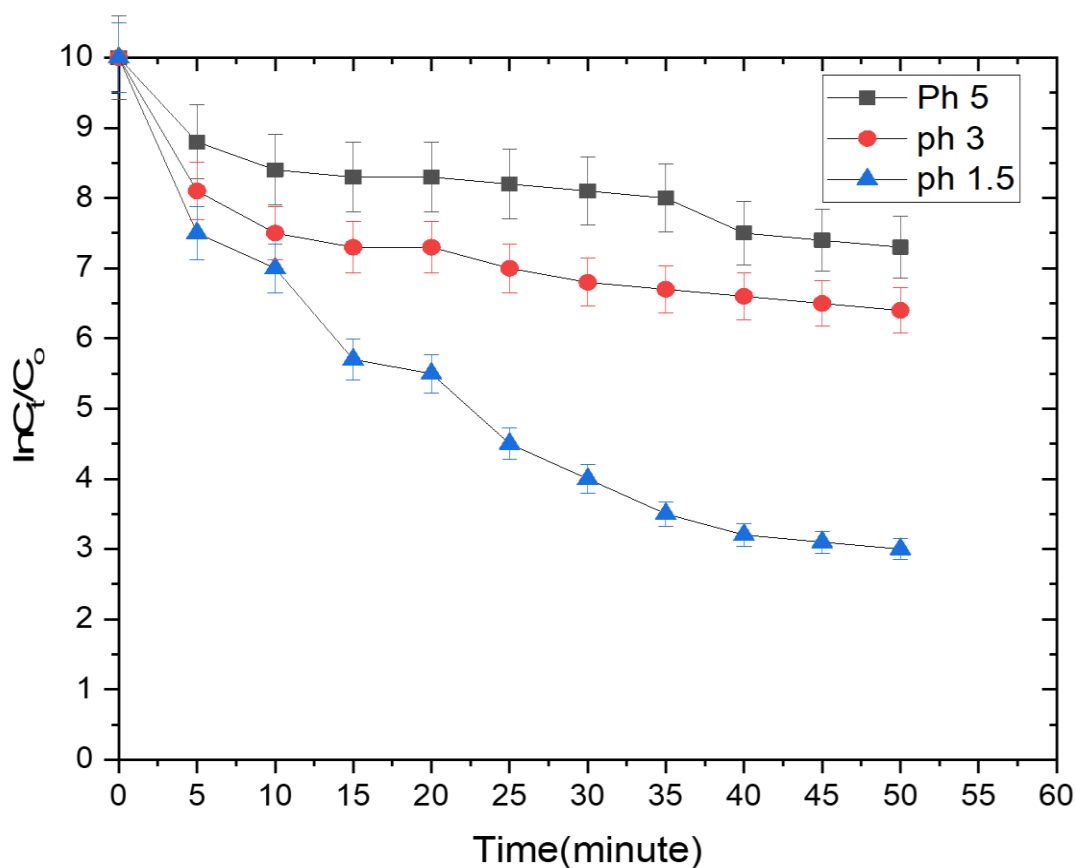| Ag/TiO$_2$ Composites	R^2	K_{app}	Reduction
0.01 Ag/TiO$_2$	0.8965	0.0259	75%
0.1 Ag/TiO$_2$	0.8708	0.014	54%
0.5 Ag/TiO$_2$	0.9243	0.0166	50%

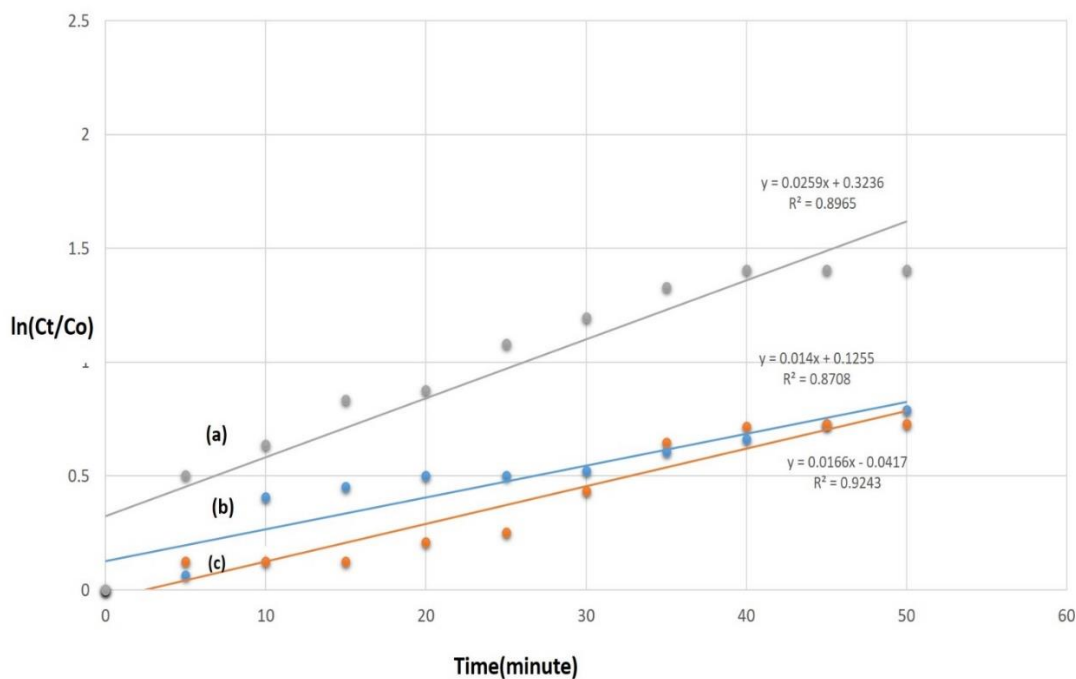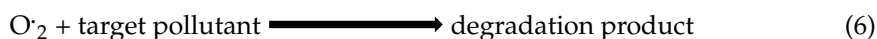**Figure 10.** Comparison graph of photocatalytic reduction of Cr (VI) to Cr (III) at different pH values.
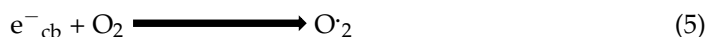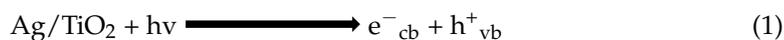

Figure 11. (**a**) The pseudo first order kinetics of 0.01Ag/TiO$_2$ composite. (**b**) The pseudo first-order kinetics of 0.1 Ag/TiO$_2$ composite. (**c**) The pseudo first-order kinetics of 0.5 Ag/TiO$_2$ composite.

The kinetics study indicates the photocatalytic reduction of Cr(VI) to Cr(III) follows the pseudo first-order reaction.

$$Ag/TiO_2 + h\nu \longrightarrow e^-_{cb} + h^+_{vb} \tag{1}$$

$$h^+vb + H_2O \longrightarrow HO + H^+ \tag{2}$$

$$HO + \text{target pollutant} \longrightarrow \text{degradation product} \tag{3}$$

$$h^+_{vb} + \text{target pollutant} \longrightarrow \text{Oxidation Product} \tag{4}$$

$$e^-_{cb} + O_2 \longrightarrow O^{\cdot}_2 \tag{5}$$

$$O^{\cdot}_2 + \text{target pollutant} \longrightarrow \text{degradation product} \tag{6}$$

$$e^-_{cb} + \text{target pollutant} \longrightarrow \text{reduction product} \tag{7}$$

The proposed mechanism of removal of photocatalytic pollutants by Ag/TiO_2 composite is shown in Figure 12. The Ag/TiO_2 in an aqueous matrix is exposed to light with an energy level over its band gap (Eg = 2.7 eV), and electrons are produced in the conduction band and holes in the valance band (Equation (1)). Hydroxyl radicals can be created when the adsorbed water reacts with the photogenerated valance band gaps (Equation (2)). Target pollutants can be subjected to a photocatalytic interaction with the generated hydroxyl radicals and the valance band holes (Equations (3) and (4)). On the other hand, the adsorbed molecular oxygen on Ag/TiO_2 can combine with the photogenerated conduction band electrons to make superoxide radical anions (Equation (5)). Moreover, the target pollutants can cause degradation and reduction products by interacting with newly formed superoxide radical anions and conduction band electrons (Equations (6) and (7)) [67].
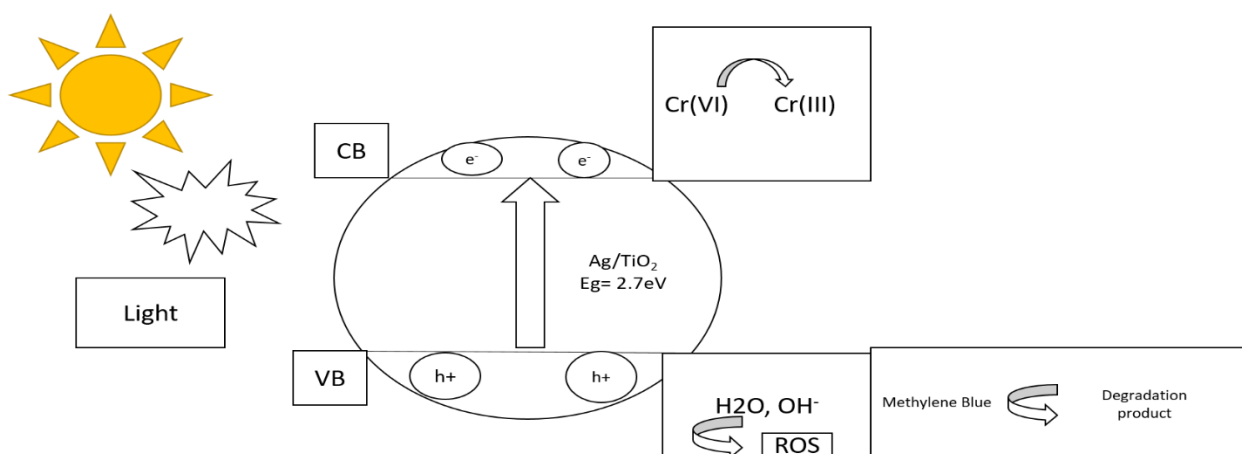

Figure 12. The simultaneous removal of photocatalytic pollutants by Ag/TiO_2 composite.

3.1. Effect of Methanol

Methanol was chosen to serve as a hole scavenger. Methanol radicals are created when the CH_3OH scavenges the h^+ in the valence band ($CH_2OH\cdot$). The hole scavenger produces a radical by removing the hydrogen from the hydroxyl group [68,69]. The valence band receives e- from the formaldehyde radicals created by the oxidation of the methanol radical. The formaldehyde undergoes additional oxidation to generate formic acid before being broken down into CO_2 and H_2O.

$$CH_3OH + h^+ \longrightarrow CH_2OH$$

$$CH_2OH^{\bullet} \longrightarrow CH_2O + H^+ + e^-$$

The conducting band can accept formaldehyde (CH_2O), H^+, and e^- as donations or fill the positively charged vacancies, which slows the rate of e^-/h^+ recombination. The produced holes are scavenged by the methanol, which is then oxidized to produce the species that donate electrons. CH_2OH. $E^o = 0.95$ V (CH_2OH/CH_2O) [70]. When a methanol hole scavenger is employed, the photogenerated holes are not immediately consumed. Instead, the hydroxyl radicals radicalize the CH_3OH, which results in the formation of e^- [71].

$$OH^\bullet + CH_3OH \longrightarrow CH_2OH^\bullet + H_2O$$

3.2. Antifungal Performance

0.01 Ag/TiO$_2$, 0.1 Ag/TiO$_2$, and 0.5 Ag/TiO$_2$ nanocomposites were further tested for their antifungal activity against *S. macrospora* and *S. maydis* using the agar well-diffusion method and amphotericin B as a reference. An overview of the findings is shown in Table 4. When compared to 0.1 Ag/TiO$_2$ and 0.5 Ag/TiO$_2$ nanocomposites, 0.01 Ag/TiO$_2$ nanocomposites display stronger toxicity, with zone inhibition values of 38.4 and 34.3 mm, as shown by the antifungal activity data (Table 4). Reduced size and the synergistic interaction of 0.01 Ag/TiO$_2$ nanocomposites resulted in an increased antifungal effect.

Table 4. Zones of inhibition for the antifungal activity of 0.01 Ag/TiO$_2$, 0.1 Ag/TiO$_2$, and 0.5 Ag/TiO$_2$ nanocomposites were determined using the Agar Well cut diffusion method.

Antifungal Performance			
Bacterial Strains	**Samples**	**Blank**	**Zone of Inhibition (mm)**
S. macrospora	0.01 Ag/TiO$_2$	0	38.4
	0.1 Ag/TiO$_2$	0	30.6
	0.5 Ag/TiO$_2$	0	27.8
S. maydis	0.01 Ag/TiO$_2$	0	34.3
	0.1 Ag/TiO$_2$	0	29.4
	0.5 Ag/TiO$_2$	0	27.2

4. Conclusions

The Ag/TiO$_2$ composites are synthesized by using the template induced method. For the crystallinity of the Ag/TiO$_2$ composites, the XRD technique is used. In contrast, the Ag/TiO$_2$ composites' morphology is determined using the SEM technique. EDS is used for element detection. Moreover, the photocatalytic removal of MB and the photocatalytic reduction of the Cr (VI) to Cr (III) are performed by using the Ag/TiO$_2$ composites as the catalysis. After performing these activities, it is concluded that 54%, 68%, and 90% methylene blue is degraded by using the 0.5 Ag/TiO$_2$, 0.1 Ag/TiO$_2$,and 0.01 Ag/TiO$_2$ composites respectively. While 50%, 54%, and 75% Cr(III) is reduced to Cr(III) by using the 0.5 Ag/TiO$_2$, 0.1 Ag/TiO$_2$, and 0.01 Ag/TiO$_2$ composites. The kinetics study shows that degradation of methylene blue follows the first-order kinetics and reduction of Cr(VI) to Cr(III) follows the pseudo first-order reaction. In both of these activities (photocatalytic degradation of methylene blue and photocatalytic reduction of Cr(VI) to Cr(III)) the best result is shown by 0.01 Ag/TiO$_2$ composite after 150 and 50 min respectively of exposure to sunlight.

Author Contributions: Methodology, M.A.; Software, A.R., S.H., H.A.I., F.F.A.-F. and E.B.E.; Validation, M.J.; Formal analysis, Z.Z., A.A. (Adnan Amjad) and A.B.; Investigation, A.A. (Ahmad Alhujaily) and S.H.; Resources, E.B.E.; Data curation, M.J.; Writing—original draft, A.R. and S.I.; Writing—review & editing, N.S.A., H.A.I. and F.F.A.-F.; Visualization, M.A.; Supervision, S.I.; Project administration, A.A. (Ahmad Alhujaily). The manuscript was written with the contributions of all authors. All authors have read and agreed to the published version of the manuscript.

References

1. Ridha, N.; Alosfur, F.; Kadhim, H.; Aboud, L.; Al-Dahan, N. Novel method to synthesis ZnO nanostructures via irradiation zinc acetate with a nanosecond laser for photocatalytic applications. *J. Mater. Sci. Mater. Electron.* **2020**, *31*, 9835–9845. [CrossRef]
2. Sher, M.; Javed, M.; Shahid, S.; Hakami, O.; Qamar, M.; Iqbal, S.; AL-Anazy, M.; Baghdadi, H.; Chemistry, P. Designing of highly active g-C_3N_4/Sn doped ZnO heterostructure as a photocatalyst for the disinfection and degradation of the organic pollutants under visible light irradiation. *J. Photochem. Photobiol.* **2021**, *418*, 113393. [CrossRef]
3. Iqbal, S.; Javed, M.; Hassan, S.; Nadeem, S.; Akbar, A.; Alotaibi, M.; Alzhrani, R.; Awwad, N.; Ibrahium, H.; Mohyuddin, A.; et al. Binary Co@ ZF/S@ GCN S-scheme heterojunction enriching spatial charge carrier separation for efficient removal of organic pollutants under sunlight irradiation. *Colloids Surf. A Physicochem. Eng. Asp* **2022**, *636*, 128177. [CrossRef]
4. Owa, F. Water pollution: Sources, effects, control and management. *Mediterr. J. Soc. Sci.* **2013**, *4*, 65. [CrossRef]
5. Manisalidis, I.; Stavropoulou, E.; Stavropoulos, A.; Bezirtzoglou, E. Environmental and health impacts of air pollution: A review. *Front. Public Health* **2020**, *8*, 14. [CrossRef]
6. Masindi, V.; Muedi, K. Environmental contamination by heavy metals. *Heavy Met.* **2018**, *10*, 115–132.
7. Ridha, N.; Alosfur, F.; Kadhim, H.; Ahmed, L. Synthesis of Ag decorated TiO_2 nanoneedles for photocatalytic degradation of methylene blue dye. *Mater. Res. Express* **2021**, *8*, 125013. [CrossRef]
8. Zhu, J.; Wu, C.; Cui, Y.; Li, D.; Zhang, Y.; Xu, J.; Li, C.; Iqbal, S.; Cao, M.; Physicochemical, S.; et al. Blue-emitting carbon quantum dots: Ultrafast microwave synthesis, purification and strong fluorescence in organic solvents. *Colloids Surf. A Physicochem. Eng. Asp.* **2021**, *623*, 126673. [CrossRef]
9. Iqbal, M.; Iqbal, S. Synthesis of stable and highly luminescent beryllium and magnesium doped ZnS quantum dots suitable for design of photonic and sensor material. *J. Lumin* **2013**, *134*, 739–746. [CrossRef]
10. Bahadur, A.; Saeed, A.; Shoaib, M.; Iqbal, S.; Anwer, S. Modulating the burst drug release effect of waterborne polyurethane matrix by modifying with polymethylmethacrylate. *J. Appl. Polym. Sci.* **2019**, *136*, 47253. [CrossRef]
11. Azam, M.; Alam, M.; Hafeez, M. Effect of tourism on environmental pollution: Further evidence from Malaysia, Singapore and Thailand. *J. Clean. Prod.* **2018**, *190*, 330–338. [CrossRef]
12. Amalanathan, M.; Parvathiraja, C.; Alothman, A.; Wabaidur, S.; Islam, M. Enhanced photocatalytic and biological observations of green synthesized AC, AC/Ag and AC/Ag/TiO_2 nanocomposites. *Res. Sq.* **2021**, 739706.
13. Šuljagić, M.; Milenković, M.; Uskoković, V.; Mirković, M.; Vrbica, B.; Pavlović, V.; Živković-Radovanović, V.; Stanković, D.; Andjelković, L. Silver distribution and binding mode as key determinants of the antimicrobial performance of iron oxide/silver nanocomposites. *Mater. Today Commun.* **2022**, *32*, 104157. [CrossRef]
14. Crini, G. Recent developments in polysaccharide-based materials used as adsorbents in wastewater treatment. *Prog. Polym. Sci.* **2005**, *30*, 38–70. [CrossRef]
15. BinSabt, M.; Sagar, V.; Singh, J.; Rawat, M.; Shaban, M. Green synthesis of CS-TiO_2 NPs for efficient photocatalytic degradation of methylene blue dye. *Polymers* **2022**, *14*, 2677. [CrossRef]
16. Bai, L.; Liu, L.; Esquivel, M.; Tardy, B.; Huan, S.; Niu, X.; Liu, S.; Yang, G.; Fan, Y.; Rojas, O. Nanochitin: Chemistry, Structure. *Assem. Appl. Chem. Rev.* **2022**, *122*, 11604–11674.
17. Sun, L.; Hu, D.; Zhang, Z.; Deng, X. Oxidative degradation of methylene blue via PDS-based advanced oxidation process using natural pyrite. *Int. J. Environ. Res. Public Health* **2019**, *16*, 4773. [CrossRef]
18. Qamar, M.; Javed, M.; Shahid, S.; Iqbal, S.; Abubshait, S.; Abubshait, H.; Ramay, S.; Mahmood, A.; Ghaithan, H. Designing of highly active g-C_3N_4/Co@ ZnO ternary nanocomposites for the disinfection of pathogens and degradation of the organic pollutants from wastewater under visible light. *J. Environ. Chem. Eng.* **2021**, *9*, 105534. [CrossRef]
19. Bahadur, A.; Shoaib, M.; Iqbal, S.; Saeed, A.; Rahman, M.; Channar, P.; Polymers, F. Regulating the anticancer drug release rate by controlling the composition of waterborne polyurethane. *React. Funct. Polym.* **2018**, *131*, 134–141. [CrossRef]
20. Alsukaibi, A. Various approaches for the detoxification of toxic dyes in wastewater. *Processes* **2022**, *10*, 1968. [CrossRef]

21. Gücek, A.; Şener, S.; Bilgen, S.; Mazmancı, M. Adsorption and kinetic studies of cationic and anionic dyes on pyrophyllite from aqueous solutions. *J. Colloid Interface Sci.* **2005**, *286*, 53–60. [CrossRef]

22. Gürses, A.; Karaca, S.; Doğar, Ç.; Bayrak, R.; Açıkyıldız, M.; Yalçın, M. Determination of adsorptive properties of clay/water system: Methylene blue sorption. *J. Colloid Interface Sci.* **2004**, *269*, 310–314. [CrossRef] [PubMed]

23. Shawabkeh, R.; Tutunji, M. Experimental study and modeling of basic dye sorption by diatomaceous clay. *Appl. Clay Sci.* **2003**, *24*, 111–120. [CrossRef]

24. Duruibe, J.; Ogwuegbu, M.; Egwurugwu, J. Heavy metal pollution and human biotoxic effects. *Int. J. Phys. Sci.* **2007**, *2*, 112–118.

25. Noreen, U.; Ahmed, Z.; Khalid, A.; Di Serafino, A.; Habiba, U.; Ali, F.; Hussain, M. Water pollution and occupational health hazards caused by the marble industries in district Mardan, Pakistan. *Environ. Technol. Innov.* **2019**, *16*, 100470. [CrossRef]

26. Sharma, P.; Singh, S.; Parakh, S.; Tong, Y. Health hazards of hexavalent chromium (Cr (VI)) and its microbial reduction. *Bioengineered* **2022**, *13*, 4923–4938. [CrossRef] [PubMed]

27. Shaibur, M. Heavy metals in chrome-tanned shaving of the tannery industry are a potential hazard to the environment of Bangladesh. *Case Stud. Chem. Environ. Eng.* **2022**, *7*, 100281. [CrossRef]

28. Cappelletti, G.; Bianchi, C.; Ardizzone, S. Nano-titania assisted photoreduction of Cr (VI): The role of the different TiO_2 polymorphs. *Appl. Catal. B Environ.* **2008**, *78*, 193–201. [CrossRef]

29. Boughriet, A.; Deram, L.; Wartel, M. Determination of dissolved chromium (III) and chromium (VI) in sea-water by electrothermal atomic absorption spectrometry. *J. Anal. At. Spectrom.* **1994**, *9*, 1135–1142. [CrossRef]

30. Jaishankar, M.; Tseten, T.; Anbalagan, N.; Mathew, B.; Beeregowda, K. Toxicity, mechanism and health effects of some heavy metals. *Interdiscip. Toxicol.* **2014**, *7*, 60. [CrossRef]

31. Wen, J.; Xue, Z.; Yin, X.; Wang, X. Insights into aqueous reduction of Cr (VI) by biochar and its iron-modified counterpart in the presence of organic acids. *Chemosphere* **2022**, *286*, 131918. [CrossRef]

32. Zhang, L.; Qiu, J.; Dai, D.; Zhou, Y.; Liu, X.; Yao, J. Cr-metal-organic framework coordination with ZnIn2S4 nanosheets for photocatalytic reduction of Cr (VI). *J. Clean. Prod.* **2022**, *341*, 130891. [CrossRef]

33. Bradberry, S.; Vale, J. Therapeutic review: Is ascorbic acid of value in chromium poisoning and chromium dermatitis? *J. Toxicol. Clin. Toxicol.* **1999**, *37*, 195–200. [CrossRef] [PubMed]

34. Velmurugan, R.; Selvam, K.; Krishnakumar, B.; Swaminathan, M. An efficient reusable and antiphotocorrosive nano ZnO for the mineralization of Reactive Orange 4 under UV-A light. *Sep. Purif. Technol.* **2011**, *80*, 119–124. [CrossRef]

35. Ma, C.-M.; Hong, G.-B.; Chen, H.-W.; Hang, N.-T.; Shen, Y.-S. Photooxidation contribution study on the decomposition of azo dyes in aqueous solutions by VUV-based AOPs. *Int. J. Photoenergy* **2011**, *2011*, 1–78. [CrossRef]

36. Bahadur, A.; Iqbal, S.; Shoaib, M.; Saeed, A. Electrochemical study of specially designed graphene-Fe_3O_4-polyaniline nanocomposite as a high-performance anode for lithium-ion battery. *Dalton Trans.* **2018**, *47*, 15031–15037. [CrossRef]

37. Koutavarapu, R.; Reddy, C.; Syed, K.; Reddy, K.; Saleh, T.; Lee, D.-Y.; Shim, J.; Aminabhavi, T. Novel Z-scheme binary zinc tungsten oxide/nickel ferrite nanohybrids for photocatalytic reduction of chromium (Cr (VI)), photoelectrochemical water splitting and degradation of toxic organic pollutants. *J. Hazard. Mater.* **2022**, *423*, 127044. [CrossRef]

38. Chakrabarti, S.; Chaudhuri, B.; Bhattacharjee, S.; Ray, A.; Dutta, B. Photo-reduction of hexavalent chromium in aqueous solution in the presence of zinc oxide as semiconductor catalyst. *Chem. Eng. J.* **2009**, *153*, 86–93. [CrossRef]

39. Al-Hamoud, K.; Shaik, M.; Khan, M.; Alkhathlan, H.; Adil, S.; Kuniyil, M.; Assal, M.; Al-Warthan, A.; Siddiqui, M.; Tahir, M. Pulicaria undulata Extract-Mediated Eco-Friendly Preparation of TiO_2 Nanoparticles for Photocatalytic Degradation of Methylene Blue and Methyl Orange. *ACS Omega* **2022**, *7*, 4812–4820. [CrossRef]

40. Gaya, U.; Abdullah, A. Heterogeneous photocatalytic degradation of organic contaminants over titanium dioxide: A review of fundamentals, progress and problems. *J. Photochem. Photobiol. C Photochem. Rev.* **2008**, *9*, 1–12. [CrossRef]

41. Mishra, S.; Chakinala, N.; Chakinala, A.; Surolia, P. Photocatalytic degradation of methylene blue using monometallic and bimetallic Bi-Fe doped TiO_2. *Catal. Commun.* **2022**, *171*, 106518. [CrossRef]

42. Ayed, S.B.; Sbihi, H.; Azam, M.; Al-Resayes, S.; Ayadi, M.; Ayari, F. Local iron ore identification: Comparison to synthesized Fe_3O_4 nanoparticles obtained by ultrasonic assisted reverse co-precipitation method for Auramine O dye adsorption. *Desalination Water Treat.* **2021**, *220*, 446–458. [CrossRef]

43. Ridha, N.; Kadhim, H.; Alosfur, F.; Ahmed, R. ZnO nanofluids prepared by laser ablation in various solvents. *Mater. Res. Express.* **2018**, *5*, 125008. [CrossRef]

44. Ridha, N.; Kadhim, H.; Alosfur, F.; Abood, L.; Madlol, R. Synthesis ZnO nanoparticles by LAL method using different energies of Nd-YAG laser. In *AIP Conference Proceedings*; AIP Publishing LLC: New York, NY, USA, 2019; p. 030026.

45. Jumali, M.H.; Noor, J.; Umar, A.; Yahya, M.; Salleh, M. Characterization of SnO_2 nanoparticles prepared by two different wet chemistry methods. *Adv. Mater. Res.* **2012**, *364*, 322–326. [CrossRef]

46. Ulhaq, I.; Ahmad, W.; Ahmad, I.; Yaseen, M.; Ilyas, M. Engineering TiO_2 supported CTAB modified bentonite for treatment of refinery wastewater through simultaneous photocatalytic oxidation and adsorption. *J. Water Process Eng.* **2021**, *43*, 102239. [CrossRef]

47. Shrestha, K.; Sorensen, C.; Klabunde, K. Synthesis of CuO nanorods, reduction of CuO into Cu nanorods, and diffuse reflectance measurements of CuO and Cu nanomaterials in the near infrared region. *J. Phys. Chem. C* **2010**, *114*, 14368–14376. [CrossRef]

48. Irimpan, L.; Krishnan, B.; Nampoori, V.; Radhakrishnan, P. Luminescence tuning and enhanced nonlinear optical properties of nanocomposites of ZnO–TiO_2. *J. Colloid Interface Sci.* **2008**, *324*, 99–104. [CrossRef]

49. Likodimos, V. Photonic crystal-assisted visible light activated TiO$_2$ photocatalysis. *Appl. Catal. B Environ.* **2018**, *230*, 269–303. [CrossRef]

50. Lee, J.-K.; Lee, Y.-J.; Chae, W.-S.; Sung, Y.-M. Enhanced ionic conductivity in PEO-LiClO 4 hybrid electrolytes by structural modification. *J. Electroceramics* **2006**, *17*, 941–944. [CrossRef]

51. Fadillah, G.; Wahyuningsih, S.; Ramelan, A. Enhanced photovoltaic performance by surface modification of TiO$_2$ nanorods with aminopropyltrimethoxysilane (APTMS). In *IOP Conference Series: Earth and Environmental Science*; IOP Publishing: Bristol, UK, 2017; p. 012005.

52. Lorenzetti, M.; Biglino, D.; Novak, S.; Kobe, S. Photoinduced properties of nanocrystalline TiO$_2$-anatase coating on Ti-based bone implants. *Mater. Sci. Eng. C* **2014**, *37*, 390–398. [CrossRef]

53. Thu, P.; Thinh, V.; Lam, V.; Bach, T.; Phong, L.; Tung, D.; Manh, D.; Van Khien, N.; Anh, T.; Le, N.T.H. Decorating of Ag and CuO on ZnO Nanowires by Plasma Electrolyte Oxidation Method for Enhanced Photocatalytic Efficiency. *Catalysts* **2022**, *12*, 801. [CrossRef]

54. Nalbandian, M.; Zhang, M.; Sanchez, J.; Kim, S.; Choa, Y.-H.; Cwiertny, D.; Myung, N. Synthesis and optimization of Ag–TiO$_2$ composite nanofibers for photocatalytic treatment of impaired water sources. *J. Hazard. Mater.* **2015**, *299*, 141–148. [CrossRef] [PubMed]

55. He, Y.; Basnet, P.; Murph, S.; Zhao, Y. Ag nanoparticle embedded TiO$_2$ composite nanorod arrays fabricated by oblique angle deposition: Toward plasmonic photocatalysis. *ACS Appl. Mater. Interfaces* **2013**, *5*, 11818–11827. [CrossRef]

56. ZMa; Guo, Q.; Mao, X.; Ren, Z.; Wang, X.; Xu, C.; Yang, W.; Dai, D.; Zhou, C.; Fan, H. Photocatalytic dissociation of ethanol on TiO$_2$ (110) by near-band-gap excitation. *J. Phys. Chem. C* **2013**, *117*, 10336–10344.

57. Wu, L.; Pei, X.; Mei, M.; Li, Z.; Lu, S. Study on Photocatalytic Performance of Ag/TiO$_2$ Modified Cement Mortar. *Materials* **2022**, *15*, 4031. [CrossRef] [PubMed]

58. Ling, L.; Feng, Y.; Li, H.; Chen, Y.; Wen, J.; Zhu, J.; Bian, Z. Microwave induced surface enhanced pollutant adsorption and photocatalytic degradation on Ag/TiO$_2$. *Appl. Surf. Sci.* **2019**, *483*, 772–778. [CrossRef]

59. Chakhtouna, H.; Benzeid, H.; Zari, N.; Qaiss, A.; Bouhfid, R. Recent progress on Ag/TiO$_2$ photocatalysts: Photocatalytic and bactericidal behaviors. *Environ. Sci. Pollut. Res.* **2021**, *28*, 44638–44666. [CrossRef]

60. Shan, R.; Lu, L.; Gu, J.; Zhang, Y.; Yuan, H.; Chen, Y.; Luo, B. Photocatalytic degradation of methyl orange by Ag/TiO$_2$/biochar composite catalysts in aqueous solutions. *Mater. Sci. Semicond. Process.* **2020**, *114*, 105088. [CrossRef]

61. Jiang, L.; Zhou, G.; Mi, J.; Wu, Z. Fabrication of visible-light-driven one-dimensional anatase TiO$_2$/Ag heterojunction plasmonic photocatalyst. *Catal. Commun.* **2012**, *24*, 48–51. [CrossRef]

62. Albiter, E.; Valenzuela, M.; Alfaro, S.; Valverde-Aguilar, G.; Martínez-Pallares, F. Photocatalytic deposition of Ag nanoparticles on TiO$_2$: Metal precursor effect on the structural and photoactivity properties. *J. Saudi Chem. Soc.* **2015**, *19*, 563–573. [CrossRef]

63. Avciata, O.; Benli, Y.; Gorduk, S.; Koyun, O. Ag doped TiO$_2$ nanoparticles prepared by hydrothermal method and coating of the nanoparticles on the ceramic pellets for photocatalytic study: Surface properties and photoactivity. *J. Eng. Technol. Appl. Sci.* **2016**, *1*, 34–50. [CrossRef]

64. Al-Mamun, M.; Karim, M.; Nitun, N.; Kader, S.; Islam, M.; Khan, M. Photocatalytic performance assessment of GO and Ag co-synthesized TiO$_2$ nanocomposite for the removal of methyl orange dye under solar irradiation. *Environ. Technol. Innov.* **2021**, *22*, 101537. [CrossRef]

65. Desai, M.; Patil, R.; Pawar, K. Selective and sensitive colorimetric detection of platinum using Pseudomonas stutzeri mediated optimally synthesized antibacterial silver nanoparticles. *Biotechnol. Rep.* **2020**, *25*, e00404. [CrossRef] [PubMed]

66. Thamaphat, K.; Limsuwan, P.; Ngotawornchai, B. Phase characterization of TiO$_2$ powder by XRD and TEM. *Agric. Nat. Resour.* **2008**, *42*, 357–361.

67. Ghanbari, S.; Givianrad, M.; Azar, P.A. Simultaneous reduction of Cr (VI) and degradation of azo dyes by F-Fe-codoped TiO$_2$/SiO$_2$ photocatalysts under visible and solar irradiation. *Can. J. Chem.* **2019**, *97*, 659–671. [CrossRef]

68. Chakrabarti, S.; Banerjee, P.; Mitra, P. Solar photocatalytic reduction of hexavalent chromium in wastewater using zinc oxide semiconductor catalyst: A comparison of performances between micro and nanoparticles. In *Physical Chemical and Biological Treatment Processes for Water and Wastewater*; Nova Science Publishers, Inc.: Hauppauge, NY, USA, 2015; p. 95À111.

69. Tan, T.; Beydoun, D.; Amal, R. Effects of organic hole scavengers on the photocatalytic reduction of selenium anions. *J. Photochem. Photobiol. A Chem.* **2003**, *159*, 273–280. [CrossRef]

70. Qamar, M.; Gondal, M.; Yamani, Z. Laser-induced efficient reduction of Cr (VI) catalyzed by ZnO nanoparticles. *J. Hazard. Mater.* **2011**, *187*, 258–263. [CrossRef]

71. Guzman, F.; Chuang, S.; Yang, C. Role of methanol sacrificing reagent in the photocatalytic evolution of hydrogen. *Ind. Eng. Chem. Res.* **2013**, *52*, 61–65. [CrossRef]